Comparable theta phase coding dynamics along the transverse axis of CA1

Aditi Bishnoi, Sachin S. Deshmukh *

Centre for Neuroscience,
Indian Institute of Science,
Bangalore

***Correspondence**
Sachin S. Deshmukh
Centre for Neuroscience,
Indian Institute of Science,
Bangalore
Email: sachin@iisc.ac.in
ORCID: AB: 0000-0001-9089-675X SSD: 0000-0002-8421-4158

Pages: 21
Figures: 6
Tables: 0
Supplementary Figures: 4
Supplementary tables: 1

Running head: Theta phase coding dynamics along the transverse axis of CA1

Author contribution

Aditi Bishnoi analyzed the data, conceived the project, and wrote the manuscript. Sachin S. Deshmukh collected the data, conceived the project, and wrote the manuscript.

Acknowledgements

We thank Jeremy Johnson, Geeta Rao, Vyash Puliyadi, Amanda Smolinsky, Lou Blanpain, and Kimberley Christian for their support in data collection; Bruce L. McNaughton for discussion; Rajat Saxena and Indraja R. Jakhalekar for inputs on the manuscript. This work was supported by Wellcome Trust/DBT India Alliance Grant IA/S/13/2/501024 and Pratiksha trust grant PE/CHAIR-19-025.03. Data collection was supported by R01 NS039456 (J. Knierim, PI).

Keywords: Hippocampus, Theta, Medial entorhinal cortex, Lateral entorhinal cortex

Comparable theta phase coding dynamics along the transverse axis of CA1

Abstract

Topographical projection patterns from the entorhinal cortex to area CA1 of the hippocampus have led to a hypothesis that proximal CA1 (pCA1) is spatially more selective than distal CA1 (dCA1). While earlier studies have shown evidence supporting this hypothesis, we recently showed that this difference does not hold true under all experimental conditions. In a complex environment with distinct local texture cues on a circular track and global visual cues, pCA1 and dCA1 display comparable spatial selectivity. Correlated with the spatial selectivity differences, the earlier studies also showed differences in theta phase coding dynamics between pCA1 and dCA1 neurons. Here we show that there are no differences in theta phase coding dynamics between neurons in these two regions under the experimental conditions where pCA1 and dCA1 neurons are equally spatially selective. We also show that dCA1 local field potentials (LFPs) show higher power in theta range compared to pCA1 LFPs. These findings challenge the established notion of dCA1 being inherently less spatially selective and theta modulated than pCA1 and suggest that theta-mediated activation of the CA1 sub-networks to represent space is task-dependent.

New and Noteworthy

Proximal CA1 has been shown to be more spatially selective and influenced by theta oscillations than distal CA1. We demonstrate an experimental condition under which this functional distinction does not persist, and distal and proximal CA1 neurons show comparable spatial selectivity and influence of theta oscillations. We discuss how the observed results cannot be explained by the anatomical segregation of the lateral and the medial entorhinal cortical inputs as proposed earlier and suggest alternative mechanisms.

Introduction

Oscillations in the theta frequency range (5-10 Hz) are prominent rhythms observed in the rodent hippocampus during REM sleep and exploratory behavior (1). These oscillations are thought to be essential for the physiological operation of the hippocampal-entorhinal complex and facilitate learning and memory (2,3). Activity of many neurons in the hippocampus and its anatomically connected regions has been shown to be modulated by theta oscillations (hippocampus: (4); entorhinal cortex: (5,6); head direction cells in the anterior thalamus: (7)). Theta oscillations provide temporal windows for coordination of neuronal responses (8-11) that can enable the efficient transfer of information within large networks and thus support learning and memory.

Spatial representations in the hippocampal-entorhinal complex are known to be associated with theta oscillations (12-13). Place cells and grid cells exhibit a temporal code for space. As the animal advances through the place or the grid field, the neurons progressively fire at earlier and earlier phases of theta oscillations (6,10,11). Certain models have proposed a role for theta oscillations in the generation of spatial code. These models use interference of two independent oscillators with different theta frequencies to generate place fields and grid fields in simulations (14-17). As theta coordinates the neural activity of spatially selective cells (18-21), studying theta oscillations and theta modulated spiking dynamics can give insights into the network computations underlying neural representations of space.

Proximal CA1 (pCA1) receives stronger projections from the medial entorhinal cortex (MEC) while distal CA1 (dCA1) receives stronger projections from the lateral entorhinal cortex (LEC) (22-25). MEC is believed to send path integration-based spatial information to the hippocampus, while LEC is believed to send sensory derived non-spatial information to the hippocampus (26-27). MEC also has stronger theta oscillations in the local field potentials (LFPs) with stronger theta modulation of principal neurons as compared to LEC (28). Following these inputs, dCA1 was predicted to be primarily involved in processing the non-spatial aspects of the environment with inherently weaker theta modulated spiking dynamics compared to pCA1, which is considered to be primarily involved in spatial information processing. Some studies have shown these predicted functional differences along the transverse axis of CA1 correlated with the topographical afferent projections from the entorhinal cortex. pCA1 pyramidal neurons have been shown to be more spatially selective and exhibit stronger spike modulation by theta oscillations than dCA1 (29-30).

Recently, we (31) reported that pCA1 and dCA1 exhibit comparable spatial selectivity on a circular track with distinct textures and multiple visual cues in the periphery. This finding raises a possibility that the differences in spatial selectivity shown in the previous studies (29,30) may not be universal, and the representation of space along the transverse axis of CA1 may change as a function of the environmental and task conditions. In the current study, we test if theta-mediated neural dynamics continue to show differences between dCA1 and pCA1 in this experimental condition where the difference in spatial selectivity disappears. In contrast to the previous reports, dCA1 exhibits theta phase precession and theta modulation comparable to pCA1. LFP theta power is higher in dCA1, while locomotion speed modulation of theta oscillation is comparable between the two sub-regions. Thus, theta-mediated spatial selectivity in CA1 may be a function of environmental complexity and task demands rather than the entorhinal cortex inputs alone.

Methods

Neurons recorded along the transverse axis of CA1 from 11 male Long Evans rats were used in this study. Data from these rats have been previously reported in (31,32). See (31) for details of the methods described briefly here. All animal procedures were performed in accordance with the National Institutes of Health (NIH) animal use guidelines and were approved by the Johns Hopkins University Animal Care and Use Committee.

Surgery

Rats were anesthetized (80mg/kg Ketamine, 10mg/kg Xylazine, and 0.4-1.5% isoflurane for maintenance) and implanted with custom-built hyperdrives over the right hemisphere. These hyperdrives, with 15 independently movable tetrodes and 2 references, had a linear bundle of canulae angled at 35° to target the entire transverse axis of dorsal CA1.

Electrophysiology recordings

An analog wireless transmitter (Triangle Biosystems International, Durham, NC) was used to collect neural data. Digitization and data processing was done using Cheetah data acquisition system (Neuralynx Inc., Bozeman, MT). The analog signals were amplified 1000-10000 fold, high pass filtered (600-6000 Hz), and digitized at 32000 Hz. Each time the signal crossed a pre-set amplitude threshold,

32 sample points were recorded around the threshold passing event (8 points before the threshold passing event and 24 points after the event at 32 KHz i.e., 1 ms) on all 4 tetrode channels as spike data. For LFP recordings, signals were digitized at 1000 Hz after amplifying 500-2000 fold and bandpass filtering between 1-475 Hz.

Animals were trained to run clockwise (CW) on a circular track while the tetrodes were moved daily to position them in the dorsal CA1 pyramidal cell layer. Once the electrodes were positioned, behavior and neural data were recorded over 5-6 sessions in the following order: STD – MIS – STD – MIS – STD for one rat and STD – STD – MIS – STD – MIS – STD for all other rats (Figure 1A), with 15 laps per session on a circular track (inner diameter: 56 cm, outer diameter: 76 cm). STD stands for the standard configuration of local and global cues, and MIS stands for mismatch configuration where the global cues along the curtain were rotated CW and local cues rotated counter-clockwise (CCW) by equal amount. The total local-global mismatch angles used for different MIS sessions were 45°, 90°, 135°, and 180°. Each mismatch angle was sampled twice over 4-6 days of recordings. First STD session of the day was used for all statistical comparisons for STD sessions reported here. The animal's position in the arena was tracked using LEDs and an overhead camera acquiring frames at 30 Hz. Timestamps where the animal was either running in the opposite direction (CCW) on the track or the animal's head was detected outside the track were removed.

Place field analysis

A custom manual cluster cutting software (WinClust, J.J. Knierim, Johns Hopkins University) was used to identify single units. Peak, valley, and energy of the spike waveforms on all 4 channels of a tetrode were used to cluster spikes. Putative interneurons with a mean firing rate of ≥ 10 Hz were excluded from further analysis.

To create a linearized firing rate map representing activity of a neuron on the track, the circular track was binned into 360 × 1° bins. The number of spikes a neuron fired while the rat occupied a particular bin was divided by the time the rat spent in that bin to obtain firing rate of that neuron in that bin. This map was smoothed for calculating spatial information score (bits/spike; (11)) using adaptive binning. The probability of obtaining the neuron's spatial information score by chance was determined using a shuffling procedure. For this, a random time lag (minimum 30 s) was added to the neuron's spike train to temporally displace it against the trajectory of the rat. An adaptive binned linearized rate map was created from this shifted spike train to compute spatial information

(11). A chance distribution of spatial information scores for the observed spike train was obtained by repeating this procedure 1000 times. The significance of the observed spatial information was determined from the chance distribution by counting the number of times the trials with random lags had spatial information scores greater than or equal to the observed score. Only putative pyramidal cells with statistically significant ($p < 0.01$) information scores > 0.5 bits/spike were used in further analysis.

Place fields were detected from Gaussian smoothed (window size = 30°, $\sigma = 9°$) linearized rate maps. Place fields were defined as having at least 10 contiguous 1° bins (corresponding to 5.7 cm at the mean diameter of the track) with firing rates ≥ 0.3 Hz and ≥ 10% of the peak firing rate for the field. Each individual place field had to have a peak firing rate ≥ 1 Hz and ≥ 30% of the overall peak firing rate of the neuron, with at least 50 spikes for the place field to be included in the analysis.

Theta detection and theta phase assignment

To obtain modulation of spiking activity by local theta oscillations, every time a neuron fired, phase of theta oscillations on the same tetrode was assigned to that spike. Peaks were detected on LFP signals filtered in the theta range (5-10 Hz) and assigned a phase of 0/360°. Each spike was assigned a phase between the consecutive peaks by linear interpolation (11). Epochs with at least 3 contiguous theta cycles, each with a peak amplitude ≥ mean + 0.8σ of the signal amplitude were identified as strong theta events. This criterion was determined by visual inspection of theta epochs to capture the strong theta events across tetrodes across rats. Only spikes that occurred during strong theta events were assigned a theta phase and included in further analysis.

Theta Phase Precession

Spike phases for two theta cycles were plotted against the position of the animal in the place field to visualize an entire cycle of phase precession. To calculate the strength of precession, the phase vector for each place field was rotated in steps of 1° with respect to the position for the entire phase cycle of 360° (10). Linear regression between phase and position was performed for each rotation. Out of the 360 linear fits, the regression line with the highest r^2 (i.e., the highest explained variance of theta phase by the position of the animal in the field) was taken as the best fit for that place field. The corresponding r^2 value was considered the strength of phase precession for that place field. Slope and range (degrees) of phase precession were also calculated for place fields that showed

significant linear regression ($p < 0.01$). Place fields with overlapping precession cycles were removed manually from further analyses (Figure S1).

Modulation of Spiking activity by local theta oscillations

Theta Modulation Index (TMI): Spike phase histograms were generated with a bin size of 36° and smoothed by a Gaussian window (window size = 7 bins, $\sigma = 0.5$ bins). TMI was defined as the peak to valley difference of the peak normalized histogram. To get a chance distribution of TMI, each spike was randomly assigned a phase value between 1° to 360° from a uniform distribution to calculate a TMI and the process was repeated for 1000 iterations. The significance of the observed TMI was determined using the proportion of random trials with TMI greater than or equal to the observed TMI. A significance threshold of $p < 0.05$ was used to identify theta modulated neurons. For performing statistics on all place cells, the place field with the highest TMI was chosen for cells with more than one place field. The same criteria of choosing the place field with the highest precession or modulation index, was used for statistical comparison on all place cells for theta phase precession and precession adjusted Theta Modulation Index, described below.

Phase Precession Adjustment of Theta Modulation Index (TMIa): To discount the influence of phase precession on TMI calculation, we measured the deviation of the spike phases from the linear phase precession fit. The deviation values could range from -360° to 360°. All negative deviation angles were converted to a 0°-360° scale by adding 360° to the negative values, and a histogram of phase deviations was generated using binning and smoothing as described for TMI. TMIa was taken as the peak to valley difference of the peak normalized phase deviation histogram. The probability of obtaining this TMIa by chance (significance criterion: $p < 0.05$) was tested against a chance distribution of TMIa. A randomized TMIa was generated by randomly assigning a phase deviation value between -360° to 360° to each spike. This process was repeated 1000 times to get a chance distribution of TMIa.

Spectral Analysis

Power Spectra were obtained from LFPs using the MATLAB *pspectrum* function. To accurately estimate the theta peak parameters from the power spectra, the $1/f^n$ component was estimated and subtracted using an open-source Python toolbox, FOOOF (33) (https://github.com/fooof-tools/fooof, release 0.1.2). The FOOOF algorithm was implemented on the power spectrum of each tetrode,

using the 'knee' parameter in the module over the frequency range of 3-100 Hz for estimating the aperiodic ($1/f^n$) fit. The $1/f^n$ 'background fit' returned by the program was subtracted from the original spectrum to obtain a 'flattened' spectrum (Figure S2). The 'flattened' spectra were used to estimate total power in the theta range (5-10 Hz) and frequency with the highest theta power.

Statistics

Projections from LEC and MEC are expected to overlap in iCA1 (22,34). Thus, iCA1 was excluded from all statistical comparisons by prior design. Non-parametric tests were used for statistical comparisons between pCA1 and dCA1: Wilcoxon signed-rank for all paired comparisons and Wilcoxon rank-sum for all unpaired comparisons.

Results

LFP and single-unit activity were recorded along the transverse axis of dorsal CA1 of 11 Long Evans rats using independently movable tetrodes. These recordings were performed as the animals ran on a circular track with four distinct textures that served as local cues and six distinct global visual cues along the surrounding circular curtain. STD sessions were interleaved with MIS sessions where the global and local cues were rotated by equal amounts in opposite directions to create cue conflict (Figure 1A). We compared theta modulated spiking dynamics between pCA1 and dCA1 neurons during STD and MIS sessions. Locations of the electrodes along the transverse axis were confirmed using histological reconstruction at the end of the experiment (Figure 1B).

Theta modulation along the transverse axis of CA1

To characterize theta modulation of spiking activity in CA1, we first identified theta events throughout a session on every electrode. LFPs from the tetrode from which a given neuron was recorded were used to measure theta oscillations local to that neuron. The phase of local theta oscillation was estimated for each spike in a neuron's place field during strong theta events (Figure 2A). A theta modulation index (TMI) was calculated for each place field of a neuron as the difference between the peak and the valley of the spike theta phase histogram normalized by the peak (Figure 2B). Only the place field with the highest TMI value was included for cells with more than one place field. We found a small but statistically significant difference in TMI of pCA1 and dCA1 (Figure 2C;

Wilcoxon rank-sum test; pCA1 median TMI = 0.69, dCA1 median TMI = 0.64; z= 2.32, ranksum = 14712, p = 0.021; pCA1 = 115 cells, dCA1 = 119 cells) but found the proportion of cells modulated by theta oscillations to be comparable between pCA1 and dCA1 (Figure 2D; chi-square test for independence; $\chi^2 = 0.085$, p = 0.77). This equal proportion of theta modulated cells in both sub-regions is in contrast with previous reports where pCA1 has been shown to have higher proportion of cells modulated by local (30) as well as MEC (29) theta oscillations compared to dCA1.

Comparable theta phase precession and precession adjusted theta modulation between pCA1 and dCA1

Hippocampal place cells often display theta phase precession by progressively shifting the theta phase in which the place cells fire as the animal passes through the neurons' place fields (Figure 3A). In contrast to the previous report from 1D environment (30), we found the strength of phase precession to be comparable between pCA1 and dCA1 cells in our experimental protocol (Figure 3B; Wilcoxon rank-sum test; pCA1 median r^2= 0.27, dCA1 median r^2 = 0.29; z = -0.73, ranksum= 13135, p = 0.466). For cells with multiple place fields, only the place field with the highest r^2 was included. A place field was considered to have significant phase precession if the linear regression fit was better than chance ($p < 0.01$). Almost all neurons in pCA1 and dCA1 showed significant theta phase precession. The proportions of cells showing significant theta phase precession were comparable in pCA1 and dCA1 (Figure 3C; chi-square test for independence; $\chi^2 = 0.004$, p = 0.947). For the theta phase precessing neurons, the dynamics of precession (slope and range of precession) also showed no significant difference between the two sub-regions (Figure 3D; Wilcoxon rank-sum test; z =1.42, ranksum=12603, p = 0.157 for slope of phase precession; z = -1.29, ranksum = 11322, p = 0.195 for range of precession).

In theta phase precession, the preferred phase of theta oscillation in which the neuron fires changes with the rat's position. Thus, the depth of the theta modulation histogram (which averages theta phases in which the neuron fires across positions) gets shallower in precessing neurons (Figure 4A). This weakens our estimate of modulation of the neuron's activity by theta oscillations using TMI. To compensate for the dependence of neuron's preferred theta phase on position and get a better estimate of its modulation by theta oscillations, we subtracted the phase precession fit from all spike theta phases in the place field. This returned deviation of theta phases from the best precession fit which was used to calculate precession adjusted TMI (TMIa) for each place field (Figure 4A). Since

precession adjustment of TMI removed the influence of spatial location on the index, it provided a better estimate of modulation of the neuron's activity by theta oscillations.

TMIa was higher than TMI for majority of place fields identified across dorsal CA1 (Figure 4B; 106 out of 125 place fields in pCA1 and 112 out of 134 place fields in dCA1, both proportions significantly greater than 50%; test for proportions; $z = 7.78$ and 7.77 for pCA1 and dCA1 respectively, $p < 0.001$ for both). Theta modulation measured using TMIa was comparable between pCA1 and dCA1 (Figure 4C; Wilcoxon rank sum test; pCA1 median TMIa= 0.84, dCA1 median TMIa = 0.82; $z = 1.3$, ranksum = 14187, $p = 0.193$) with similar proportion of cells being significantly theta modulated after adjustment for precession (Figure 4D; chi-square test for independence; $\chi^2 = 0.68$, $p = 0.407$). Notice how the small but statistically significant difference in TMI ($p = 0.021$; Figure 2) reported earlier in the results disappears after adjusting for phase precession (TMIa: $p = 0.193$), removing any uncertainties about whether there is a difference in influence of theta oscillations on neural activity in pCA1 and dCA1.

Similar trends were observed during the MIS sessions. The strength of phase precession was comparable between pCA1 and dCA1 for all MIS sessions (Figure 5A; Wilcoxon rank-sum; $p > 0.1$; Supplementary Table 1). TMIa were higher than TMI for most place fields recorded in different MIS sessions (Figure 5B; proportions significantly greater than 50% for all MIS sessions; test for proportions, $p < 0.001$ for all MIS sessions for both pCA1 and dCA1; see Supplementary Table 1 for detailed statistics). For statistical comparisons on all place cells, only the place field with the highest TMIa was included for cells with multiple place fields. TMIa also showed no significant difference between the two sub-regions for three out of four MIS sessions (Figure 5C; Wilcoxon rank-sum; $p < 0.05$ only for MIS 45°; Supplementary Table 1). Similar proportions of place cells in pCA1 and dCA1 were significantly theta modulated during all MIS sessions (Figure 5D; chi-square test for independence; $p > 0.1$ for all MIS sessions; Supplementary Table 1). The cell populations of pCA1 and dCA1 included in all the statistical comparisons were not independently sampled in STD and different MIS sessions. As correction for multiple comparisons cannot be performed on samples that are not independent, the p values from single sessions here cannot be interpreted in isolation. However, trends across sessions are informative. The overall trend across STD and MIS sessions shows theta phase coding dynamics to be similar along the CA1 transverse axis in our experimental protocol. This observation is consistent with the previously reported observation of comparable spatial selectivity between pCA1 and dCA1 in the same experimental protocol (31).

LFP theta power is higher in dCA1 than pCA1

Slow oscillations in the LFP permit the integration of neural responses over long time windows and allow synchronization of neural activity over distributed brain regions (2). The power of theta oscillations in LFP can be used to study the contribution of synchronized neural responses to the local network activity (2,35,36). To check if pCA1 and dCA1 networks showed differences in the strength of theta synchronized local activity, we looked at total power in the theta frequency range along the CA1 transverse axis. The power spectrum of each tetrode, after removing the $1/f^n$ component, was normalized by the highest power in the theta range across all tetrodes within a rat. Theta peak frequency and total power in the theta range for each region (pCA1, iCA1 and dCA1) for the given rat was determined from the means of the normalized power spectra of all tetrodes in the given region (Figure 6A, S3). Since theta amplitude and phase are known to change along with the depth of the electrode within CA1 (35), we analyzed LFP theta power and theta peak frequency only for the tetrodes which were in the pyramidal cell layer on the day of recording, as confirmed from the putative pyramidal cell spiking activity. To avoid oversampling the same region, data from a day with the maximum number of tetrodes recording pyramidal cell activity during a session was chosen from each rat to perform the statistics.

Out of the 11 rats included in this study, 10 had tetrodes recording pyramidal cell activity in both pCA1 and dCA1. In all rats, we found that dCA1 had higher theta power than pCA1 in the STD session (Figure 6B; Wilcoxon signed rank; $W = 0$, $p = 0.002$, $n = 10$ rats. The proportion, 10/10 rats, was significantly greater than the chance proportion of 0.5; test for proportions, $z = 3.16$, $p < 0.001$). The peak theta frequencies in pCA1 and dCA1 were statistically indistinguishable (Wilcoxon signed rank test; $W = 1.5$, $p = 1$). A similar trend of higher theta power in dCA1 than pCA1 was observed in all MIS sessions (Figure 6C; Wilcoxon signed rank; $p < 0.01$ for all MIS sessions, see Supplementary Table 1). 8/11 rats were included for MIS 90° and 9/11 rats were included for MIS 45°,135°, 180°, after ensuring every rat had at least one tetrode each in the pCA1 and dCA1 pyramidal cell layer. All rats continued to show greater theta power in dCA1 than pCA1 in MIS 45° and 90° sessions (the proportions 9/9 rats and 8/8 rats are significantly greater than the chance proportion of 0.5; test for proportions, $z = 3$, $p = 0.001$ and $z = 2.82$, $p = 0.002$, respectively); all except one rat continued to show greater theta power in dCA1 than pCA1 in MIS 135°and 180° sessions (the proportion 8/9 rats is significantly greater than the chance proportion of 0.5; test for proportions, $z = 2.33$, $p = 0.01$). The peak theta frequencies in pCA1 and dCA1 were statistically indistinguishable in all MIS sessions (data not shown, statistics in Supplementary Table 1).

Theta oscillation amplitude and frequency in different parts of the entorhinal-hippocampal complex are known to vary with the animal's speed (37-39). Speed modulation of CA1 theta amplitude and theta frequency was observed in our experimental protocol but did not show any significant differences between pCA1 and dCA1 (Figure S4).

Discussion

Comparison with the previous reports of theta dynamics and spatial selectivity along the transverse axis of CA1

Based on anatomical connectivity patterns, MEC is thought to be a part of the dorsal "where" stream, while LEC is thought to be a part of the ventral "what" stream (40-42). MEC and LEC project differentially along the transverse axis of CA1. MEC projects more strongly to pCA1 than dCA1, while LEC projects more strongly to dCA1 than pCA1 (22-25). Correlated with strong theta modulated path integration based inputs from MEC, higher spatial selectivity and theta modulation have been shown in pCA1 compared to dCA1 (29,30,43).

In this paper, we have demonstrated that pyramidal cells in dCA1 and pCA1 show comparable theta phase precession and theta modulation when the rats run on a circular track with 4 distinct local textures in the presence of multiple global cues. An identical proportion of spatially selective cells in dCA1 and pCA1 exhibit theta modulation and theta phase precession suggesting comparable levels of theta mediated activation along the transverse axis of CA1 in representing this cue-rich environment. In addition, dCA1 shows higher power in LFP theta oscillations than pCA1. This work complements our earlier report that in the same experimental protocol, dCA1 and pCA1 have comparable spatial selectivity (31). These results indicate that the previously reported lower spatial selectivity and correspondingly lower theta modulation and theta phase precession in dCA1 than pCA1 (29,30) are not immutable, and experimental conditions and/or task demands may alter the balance. In our experimental protocol, LEC is non-selective to space (44) and has very weak theta power and theta modulation (28). Thus, the change in the functionality of dCA1 from the previously reported simple environments to the more complex environment reported here cannot be explained as being caused by stronger sensory derived spatial and theta modulated/precessing inputs from LEC in the presence of distinct textures on the track.

Responses of pCA1 and dCA1 to the cue-mismatch manipulations need to be considered before proposing plausible mechanisms for the above results. Theta modulation and theta phase precession were found to be comparable between pCA1 and dCA1 for almost all cue configurations across different STD and MIS sessions. We have previously reported that dCA1 spatial representation rotates coherently with global cues from STD to MIS sessions, while pCA1 representation loses coherence (31). Loss of coherence in pCA1 can be explained by strong competing inputs it receives – MEC representation rotates with global cues (45), while distal CA3 representation rotates with local cues (46). In contrast, neither LEC (45) nor proximal CA3 (46) show coherent rotation with global cues. We (31) proposed that in the absence of strong competing inputs, the less numerous inputs from MEC (25,45), subiculum (47-49), and nucleus reuniens (50-54) may be sufficient to drive dCA1 to rotate coherently with the global cues. While these inputs might be sufficient to explain the responses along the transverse axis of CA1 to cue mismatch, additional mechanisms must be considered to explain comparable spatial selectivity in pCA1 and dCA1 in our task (31) in contrast to the previous reports (29,30). Spatial selectivity of the MEC/subiculum/nucleus reuniens inputs may be higher in our complex environment than in the previous simple environments. Alternatively, excitability in dCA1 may increase in response to higher task demand (31).

Can these mechanisms proposed to explain the patterns of spatial selectivity and coherence of responses to cue manipulation along the transverse axis of CA1 also explain the difference in theta phase precession and modulation between the previous reports (29,30) and the present study? Spatially selective inputs from MEC/subiculum/nucleus reuniens are theta modulated (6-7,52-53,55-56). An increase in their theta modulation and/or spatially selective response amplitude may result in higher theta responsivity in dCA1 in the present task. Alternatively, an increase in theta drive onto dCA1 from the pacemaker, the medial septum (37,57-59), in the present task may explain our results. To the best of our knowledge, the medial septum does not show differential projection patterns along the transverse axis of CA1, and we do not know if the pacemaker inputs to pCA1 and dCA1 can be differentially modulated. Thirdly, neuromodulatory inputs may increase the excitability of dCA1 neurons in the present task compared to the previous reports (29,30). Such increase in excitability can lead to both increased spatial selectivity as well as increased theta oscillatory dynamics in dCA1 by making it more responsive to inputs from MEC/subiculum/nucleus reuniens and the medial septum, eliminating the need for the differential modulation of these inputs. Lastly, the spatially nonselective inputs from LEC (44) are not theta modulated (28) and rotate weakly with the local cues (45) in the present task. These LEC inputs cannot explain the coherent rotation of dCA1 with global cues. However, higher firing rates of LEC neurons in the present task compared to

the previous reports may lead to increased theta oscillatory dynamics as well as spatial selectivity in dCA1. Higher activity of nonspatial non-theta-modulated LEC inputs may lead to the dCA1 neurons being closer to the action potential threshold, effectively increasing their excitability, and thus giving rise to more robust responses to spatially selective as well as theta oscillatory inputs. Experiments explicitly comparing the activity of pCA1 and dCA1 neurons as well as their inputs in environments of different levels of complexity and task demands, beyond the scope of the present work, are necessary to disambiguate between these plausible mechanisms.

LFP theta power in pCA1 and dCA1

LFPs in dCA1 show stronger theta oscillations than pCA1 in our experimental protocol. Previous studies (29,30) did not compare amplitudes of theta oscillations in pCA1 and dCA1 LFPs. Hence, we do not know if the relative theta power in dCA1 and pCA1 changes from the previous studies to the present study. The observed difference in the amplitude of the LFP theta oscillations between pCA1 and dCA1 could be caused by a variety of factors such as morphology and density of the pyramidal cells, laminar organization and density of their inputs, local curvature, etc. (35,36). Speed modulation of theta oscillations is comparable in pCA1 and dCA1. Thus, the difference in theta power in LFP may not be caused by pCA1 and dCA1 theta generators being differentially modulated by speed. Higher theta power in dCA1 LFPs than pCA1 LFPs, together with comparable strength of theta modulation between dCA1 and pCA1 neurons, suggests that theta oscillations can drive the dCA1 network at least as strongly as the pCA1 network under certain task conditions.

Summary

Our study, together with (31), challenges the notion that dCA1 is inherently less spatial and has weaker theta oscillatory dynamics than pCA1. We suggest that LEC and MEC drives onto dCA1 and pCA1 respectively are not nearly as mutually exclusive as suggested earlier, and their relative contributions may change based on task demands. Further experiments are necessary to discern relative contributions of inputs beyond LEC and MEC to functional differences along the transverse axis of CA1 and their task dependent modulation.

References

1. **Vanderwolf CH**. Hippocampal electrical activity and voluntary movement in the rat. *Electroencephalogr Clin Neurophysiol* 26: 407–418, 1969.doi: 10.1016/0013-4694(69)90092-3

2. **Colgin LL**. Mechanisms and Functions of Theta Rhythms. *Annual Review of Neuroscience* 36: 295–312, 2013. doi: 10.1146/annurev-neuro-062012-170330.

3. **Nuñez A**, **Buño W**. The Theta Rhythm of the Hippocampus: From Neuronal and Circuit Mechanisms to Behavior. *Frontiers in Cellular Neuroscience* 15: 31, 2021. doi: 10.3389/fncel.2021.649262.

4. **Ranck JB**. Studies on single neurons in dorsal hippocampal formation and septum in unrestrained rats: Part I. Behavioral correlates and firing repertoires. *Experimental Neurology* 41: 462–531, 1973. doi: 10.1016/0014-4886(73)90290-2.

5. **Alonso A**, **García-Austt E**. Neuronal sources of theta rhythm in the entorhinal cortex of the rat. *Exp Brain Res* 67: 493–501, 1987. doi: 10.1007/BF00247282.

6. **Hafting T**, **Fyhn M**, **Bonnevie T**, **Moser M-B**, **Moser EI**. Hippocampus-independent phase precession in entorhinal grid cells. *Nature* 453: 1248–1252, 2008. doi: 10.1038/nature06957.

7. **Tsanov M**, **Chah E**, **Vann SD**, **Reilly RB**, **Erichsen JT**, **Aggleton JP**, **O'Mara SM**. Theta-Modulated Head Direction Cells in the Rat Anterior Thalamus. *J Neurosci* 31: 9489–9502, 2011. doi: 10.1523/JNEUROSCI.0353-11.2011.

8. **Jones MW**, **Wilson MA**. Theta Rhythms Coordinate Hippocampal–Prefrontal Interactions in a Spatial Memory Task. *PLOS Biology* 3: e402, 2005. doi: 10.1371/journal.pbio.0030402.

9. **Mizuseki K**, **Sirota A**, **Pastalkova E**, **Buzsáki G**. Theta Oscillations Provide Temporal Windows for Local Circuit Computation in the Entorhinal-Hippocampal Loop. *Neuron* 64: 267–280, 2009. doi: 10.1016/j.neuron.2009.08.037.

10. **O'Keefe J**, **Recce ML**. Phase relationship between hippocampal place units and the EEG theta rhythm. *Hippocampus* 3: 317–330, 1993. doi: https://doi.org/10.1002/hipo.450030307.

11. **Skaggs WE**, **McNaughton BL**, **Wilson MA**, **Barnes CA**. Theta phase precession in hippocampal neuronal populations and the compression of temporal sequences. *Hippocampus* 6: 149–172, 1996. doi: 10.1002/(SICI)1098-1063(1996)6:2<149::AID-HIPO6>3.0.CO;2-K.

12. **Buzsáki G**, **Moser EI**. Memory, navigation and theta rhythm in the hippocampal-entorhinal system. *Nat Neurosci* 16: 130–138, 2013. doi: 10.1038/nn.3304.

13. **Mitchell SJ**, **Rawlins JN**, **Steward O**, **Olton DS**. Medial septal area lesions disrupt theta rhythm and cholinergic staining in medial entorhinal cortex and produce impaired radial arm maze behavior in rats. *J Neurosci* 2: 292–302, 1982. doi: 10.1523/JNEUROSCI.02-03-00292.1982.

14. **O'Keefe J**, **Burgess N**. Dual phase and rate coding in hippocampal place cells: Theoretical significance and relationship to entorhinal grid cells. *Hippocampus* 15: 853–866, 2005. doi: 10.1002/hipo.20115.

15. **Burgess N**. Grid cells and theta as oscillatory interference: Theory and predictions. *Hippocampus* 18: 1157–1174, 2008. doi: 10.1002/hipo.20518.

16. **Burgess N**, **O'Keefe J**. Models of place and grid cell firing and theta rhythmicity. *Current Opinion in Neurobiology* 21: 734–744, 2011. doi: 10.1016/j.conb.2011.07.002.

17. **Barry C**, **Bush D**, **O'Keefe J**, **Burgess N**. Models of grid cells and theta oscillations. *Nature* 488: E1–E1, 2012. doi: 10.1038/nature11276.

18. **Lisman JE**, **Talamini LM**, **Raffone A**. Recall of memory sequences by interaction of the dentate and CA3: A revised model of the phase precession. *Neural Networks* 18: 1191–1201, 2005. doi: 10.1016/j.neunet.2005.08.008.

19. **Maurer AP**, **Cowen SL**, **Burke SN**, **Barnes CA**, **McNaughton BL**. Organization of hippocampal cell assemblies based on theta phase precession. *Hippocampus* 16: 785–794, 2006. doi: 10.1002/hipo.20202.

20. **Foster DJ**, **Wilson MA**. Hippocampal theta sequences. *Hippocampus* 17: 1093–1099, 2007. doi: 10.1002/hipo.20345.

21. **Wang Y**, **Romani S**, **Lustig B**, **Leonardo A**, **Pastalkova E**. Theta sequences are essential for internally generated hippocampal firing fields. *Nat Neurosci* 18: 282–288, 2015. doi: 10.1038/nn.3904.

22. **Steward O**, **Scoville SA**. Cells of origin of entorhinal cortical afferents to the hippocampus and fascia dentata of the rat. *J Comp Neurol* 169: 347–370, 1976. doi: 10.1002/cne.901690306.

23. **Witter MP**, **Amaral DG**. Hippocampal Formation. In: *The Rat Nervous System*. Elsevier Inc., 2004, p. 635-704. doi: 10.1016/B978-012547638-6/50022-5.

24. **Ito HT**, **Schuman EM**. Functional division of hippocampal area CA1 via modulatory gating of entorhinal cortical inputs. *Hippocampus* 22: 372–387, 2011. doi: 10.1002/hipo.20909.

25. **Masurkar AV**, **Srinivas KV**, **Brann DH**, **Warren R**, **Lowes DC**, **Siegelbaum SA**. Medial and Lateral Entorhinal Cortex Differentially Excite Deep versus Superficial CA1 Pyramidal Neurons. *Cell Rep* 18: 148–160, 2017. doi: 10.1016/j.celrep.2016.12.012.

26. **Burwell RD**, **Amaral DG**. Cortical afferents of the perirhinal, postrhinal, and entorhinal cortices of the rat. *J Comp Neurol* 398: 179–205, 1998. doi: 10.1002/(sici)1096- 9861(19980824) 398:2 <179::aid-cne3>3.0.co;2-y

27. **Hargreaves EL**, **Rao G**, **Lee I**, **Knierim JJ**. Major Dissociation Between Medial and Lateral Entorhinal Input to Dorsal Hippocampus. *Science* 308: 1792–1794, 2005. doi: 10.1126/science.1110449.

28. **Deshmukh SS**, **Yoganarasimha D**, **Voicu H**, **Knierim JJ**. Theta Modulation in the Medial and the Lateral Entorhinal Cortices. *J Neurophysiol* 104: 994–1006, 2010. doi: 10.1152/jn.01141.2009.

29. **Henriksen EJ**, **Colgin LL**, **Barnes CA**, **Witter MP**, **Moser M-B**, **Moser EI**. Spatial Representation along the Proximodistal Axis of CA1. *Neuron* 68: 127–137, 2010. doi: 10.1016/j.neuron.2010.08.042.

30. **Oliva A**, **Fernández-Ruiz A**, **Buzsáki G**, **Berényi A**. Spatial coding and physiological properties of hippocampal neurons in the Cornu Ammonis subregions. *Hippocampus* 26: 1593–1607, 2016. doi: 10.1002/hipo.22659.

31. **Deshmukh SS**. Distal CA1 maintains a more coherent spatial representation than proximal CA1 when local and global cues conflict. *J Neurosci* 41: 9767-9781, 2021. doi: 10.1523/JNEUROSCI.2938-20.2021

32. **Kumar M**, **Deshmukh SS**. Differential propagation of ripples along the proximodistal and septotemporal axes of dorsal CA1 of rats. *Hippocampus* 30: 970–986, 2020. doi: 10.1002/hipo.23211.

33. **Donoghue T**, **Haller M**, **Peterson EJ**, **Varma P**, **Sebastian P**, **Gao R**, **Noto T**, **Lara AH**, **Wallis JD**, **Knight RT**, **Shestyuk A**, **Voytek B**. Parameterizing neural power spectra into periodic and aperiodic components. *Nature Neuroscience* 23: 1655–1665, 2020. doi: 10.1038/s41593-020-00744-x.

34. **Steward O**. Topographic organization of the projections from the entorhinal area to the hippocampal formation of the rat. *J Comp Neurol* 167: 285–314, 1976. doi: 10.1002/cne.901670303.

35. **Buzsáki G**. Theta Oscillations in the Hippocampus. *Neuron* 33: 325–340, 2002. doi: 10.1016/S0896-6273(02)00586-X.

36. **Buzsáki G**, **Anastassiou CA**, **Koch C**. The origin of extracellular fields and currents — EEG, ECoG, LFP and spikes. *Nat Rev Neurosci* 13: 407–420, 2012. doi: 10.1038/nrn3241.

37. **Bland BH**, **Oddie SD**. Theta band oscillation and synchrony in the hippocampal formation and associated structures: the case for its role in sensorimotor integration. *Behavioural Brain Research* 127: 119–136, 2001. doi: 10.1016/S0166-4328(01)00358-8.

38. **Hinman JR**, **Penley SC**, **Long LL**, **Escabí MA**, **Chrobak JJ**. Septotemporal variation in dynamics of theta: speed and habituation. *Journal of Neurophysiology* 105: 2675–2686, 2011. doi: 10.1152/jn.00837.2010.

39. **Long LL**, **Hinman JR**, **Chen C-M**, **Escabi MA**, **Chrobak JJ**. Theta Dynamics in Rat: Speed and Acceleration across the Septotemporal Axis. *PLOS ONE* 9: 11, 2014. doi: 10.1371/journal.pone.0097987

40. **Mishkin M**, **Ungerleider LG**, **Macko KA**. Object vision and spatial vision: two cortical pathways. *Trends in Neurosciences* 6: 414–417, 1983. doi: 10.1016/0166-2236(83)90190-X.

41. **Suzuki WA**, **Amaral DG**. Perirhinal and parahippocampal cortices of the macaque monkey: cortical afferents. *J Comp Neurol* 350: 497–533, 1994. doi: 10.1002/cne.903500402.

42. **Knierim JJ**, **Neunuebel JP**, **Deshmukh SS**. Functional correlates of the lateral and medial entorhinal cortex: objects, path integration and local–global reference frames. *Phil Trans R Soc B* 369: 20130369, 2014. doi: 10.1098/rstb.2013.0369.

43. **Igarashi KM**, **Ito HT**, **Moser EI**, **Moser M-B**. Functional diversity along the transverse axis of hippocampal area CA1. *FEBS Letters* 588: 2470–2476, 2014. doi: 10.1016/j.febslet.2014.06.004.

44. **Yoganarasimha D**, **Rao G**, **Knierim JJ**. Lateral entorhinal neurons are not spatially selective in cue-rich environments. *Hippocampus* 21: 1363–1374, 2011. doi: 10.1002/hipo.20839.

45. **Neunuebel JP**, **Yoganarasimha D**, **Rao G**, **Knierim JJ**. Conflicts between Local and Global Spatial Frameworks Dissociate Neural Representations of the Lateral and Medial Entorhinal Cortex. *Journal of Neuroscience* 33: 9246–9258, 2013. doi: 10.1523/JNEUROSCI.0946-13.2013.

46. **Lee H**, **Wang C**, **Deshmukh SS**, **Knierim JJ**. Neural Population Evidence of Functional Heterogeneity along the CA3 Transverse Axis: Pattern Completion versus Pattern Separation. *Neuron* 87: 1093–1105, 2015. doi: 10.1016/j.neuron.2015.07.012.

47. **Ding S-L**. Comparative anatomy of the prosubiculum, subiculum, presubiculum, postsubiculum, and parasubiculum in human, monkey, and rodent. *J Comp Neurol* 521: 4145–4162, 2013. doi: 10.1002/cne.23416.

48. **Xu X**, **Sun Y**, **Holmes TC**, **López AJ**. Noncanonical connections between the subiculum and hippocampal CA1. *J Comp Neurol* 524: 3666–3673, 2016. doi: 10.1002/cne.24024.

49. **Sharma A**, **Nair I**, **Doreswamy Y**. Attractor-like spatial representations in the Subicular Complex network, *bioRxiv*, 2020.doi: 10.1101/2020.02.05.935379

50. **Dolleman-Van Der Weel MJ**, **Witter MP**. Projections from the nucleus reuniens thalami to the entorhinal cortex, hippocampal field CA1, and the subiculum in the rat arise from different populations of neurons. *J Comp Neurol* 364: 637–650, 1996. doi: 10.1002/(SICI)1096-9861(19960122)364:4<637::AID-CNE3>3.0.CO;2-4.

51. **Vertes RP**, **Hoover WB**, **Do Valle AC**, **Sherman A**, **Rodriguez JJ**. Efferent projections of reuniens and rhomboid nuclei of the thalamus in the rat. *J Comp Neurol* 499: 768–796, 2006. doi: 10.1002/cne.21135.

52. **Jankowski MM**, **Islam MN**, **Wright NF**, **Vann SD**, **Erichsen JT**, **Aggleton JP**, **O'Mara SM**. Nucleus reuniens of the thalamus contains head direction cells. *eLife* 3, 2014. doi: 10.7554/eLife.03075.

53. **Jankowski MM**, **Passecker J**, **Islam MN**, **Vann S**, **Erichsen JT**, **Aggleton JP**, **O'Mara SM**. Evidence for spatially-responsive neurons in the rostral thalamus. *Front Behav Neurosci* 9, 2015. doi: 10.3389/fnbeh.2015.00256.

54. **Dolleman-van der Weel MJ**, **Griffin AL**, **Ito HT**, **Shapiro ML**, **Witter MP**, **Vertes RP**, **Allen TA**. The nucleus reuniens of the thalamus sits at the nexus of a hippocampus and medial prefrontal cortex circuit enabling memory and behavior. *Learn Mem* 26: 191–205, 2019. doi: 10.1101/lm.048389.118.

55. **Cacucci F**, **Lever C**, **Wills TJ**, **Burgess N**, **O'Keefe J**. Theta-Modulated Place-by-Direction Cells in the Hippocampal Formation in the Rat. *J Neurosci* 24: 8265–8277, 2004. doi: 10.1523/JNEUROSCI.2635-04.2004.

56. **Poulter S**, **Lee SA**, **Dachtler J**, **Wills TJ**, **Lever C**. Vector trace cells in the subiculum of the hippocampal formation. *Nature Neuroscience* 24: 266–275, 2021. doi: 10.1038/s41593-020-00761-w.

57. **Petsche H**, **Stumpf C**, **Gogolak G**. The significance of the rabbit's septum as a relay station between the midbrain and the hippocampus. I. The control of hippocampus arousal activity by the septum cells. *Electroencephalogr Clin Neurophysiol* 14: 202–211, 1962. doi: 10.1016/0013-4694(62)90030-5.

58. **Gaykema RPA**, **Luiten PGM**, **Nyakas C**, **Traber J**. Cortical projection patterns of the medial septum-diagonal band complex. *J Comp Neurol* 293: 103–124, 1990. doi: 10.1002/cne.902930109.

59. **Koenig J**, **Linder AN**, **Leutgeb JK**, **Leutgeb S**. The Spatial Periodicity of Grid Cells Is Not Sustained During Reduced Theta Oscillations. *Science* 332: 592–595, 2011. doi: 10.1126/science.1201685.

Figure Legends

Figure 1. Experimental protocol and recording locations. (A) Local and global cue mismatch protocol. Four different textures were used as local cues on the circular track; six global cues were placed along the curtain represented by a black circle around the track, either on the floor or hung from the ceiling. Rats were trained to run CW on the circular track. STD sessions where the local and global cues were maintained in their familiar configuration were interleaved with MIS sessions where the local cues were rotated CCW, and global cues were rotated CW by equal amount. Mismatch angles of 45°, 90°, 135°, or 180° were pseudorandomly selected for a particular MIS session to sample each mismatch angle twice over 4 days of experiments. The arrangement of cues for MIS 180° and MIS 90° is shown here. The arrow marks the order in which the sessions were recorded. **(B)** Coronal sections showing examples of recording locations along the transverse axis of CA1. White circles highlight the example tetrode tracks; red lines mark the CA1 boundaries. Top: an example of a tetrode in pCA1, Middle: iCA1, Bottom: dCA1.

Figure 2. Theta modulation. (A) Example raw LFP trace (top) and corresponding filtered signal (bottom). Vertical red lines represent spikes from one of the neurons that were isolated on the same tetrode. **(B)** Calculation of Theta Modulation index (TMI) for the neuron shown in A from its spike

phase histogram for 2 cycles of theta oscillation. **(C)** Box and whisker plots of the distribution of TMI for all place cells recorded in STD session show that dCA1 and pCA1 have comparable TMI. Medians are represented by horizontal lines in each box. Each box spans from the 25th to the 75th percentile (the difference is the interquartile range- IQR). Outliers, marked with red crosses, are values more than 1.5 times the IQR away from the top or bottom of the box. Whiskers extend above and below each box marking the range between the non-outlier maximum and the non-outlier minimum. **(D)** Proportion of cells with significant TMI in at least one of their place fields were similar in pCA1 and dCA1 (numbers inside bars indicate numbers of cells with significant TMI and the total number of cells).

Figure 3. Theta phase precession. (A) Example cells from each region along the CA1 transverse axis showing theta phase precession. For each cell, top trace: firing rate of the cell as a function of position on the linearized circular track. Black lines below the rate map mark the detected place field. Bottom: scatter plot of spike theta phases as a function of the position of the animal in the place field. Position in the place field has been normalized for display purposes. 0 and 1 mark the beginning and end of the place field, respectively. **(B)** Box and whisker plots showing the distribution of precession strength (r^2, i.e. the variance in spike phase explained by position in the place field) for all place cells recorded in STD session. **(C)** Proportion of cells with significant theta phase precession in at least one of their place fields. **(D)** Slope and range of phase precession for the cells showing phase precession.

Figure 4. Phase precession adjusted TMI. (A) Examples showing estimation of theta modulation before and after adjusting for theta phase precession. **Left**: example place field with strong precession (statistically significant high r^2) but low TMI. From top to bottom: spike phase histograms for all spikes in a place field, linear fit for phase precession, deviation of phases from the phase precession linear fit, and the histogram of these deviation angles used to calculate the phase precession adjusted TMI (TMIa). **Right:** place field of another cell with TMI close to the median TMI and weak precession (statistically significant low r^2). **(B)** Scatter plots of TMIa vs. TMI. Each dot represents an individual place field; filled dots represent place fields with significant TMIa. Notice how most of the dots lie above the identity line. **(C)** Box and whisker plots showing the distribution of TMIa for all place cells. Theta modulation after precession adjustment was comparable between pCA1 and dCA1. **(D)** Proportion of cells with significant TMIa in at least one of their place fields modulated by theta oscillations.

Figure 5. Theta phase coding during MIS sessions. Each column corresponds to a single MIS angle shown at the top of each column. **(A)** Distribution of theta phase precession strength. **(B)** Scatter plots of TMIa vs. TMI. **(C)** Distribution of TMIa. **(D)** Proportion of cells with significant TMIa in at least one of their place fields modulated by theta oscillations.

Figure 6. Theta power along the CA1 transverse axis. (A) Left: example power spectra of individual tetrodes from one rat normalized by the maximum power in the theta range. **Right:** average power spectra in the theta range of pCA1, iCA1, and dCA1 tetrodes for each rat for STD session **(B)** Total power in the theta range (top) and peak theta frequency (bottom) in STD session across all rats (rats represented as dots by the same color as in the right plot in (A)) **(C)** Total power in the theta range for MIS sessions. Across STD and MIS sessions, dCA1 LFPs tended to have higher power in theta range than pCA1 LFPs.

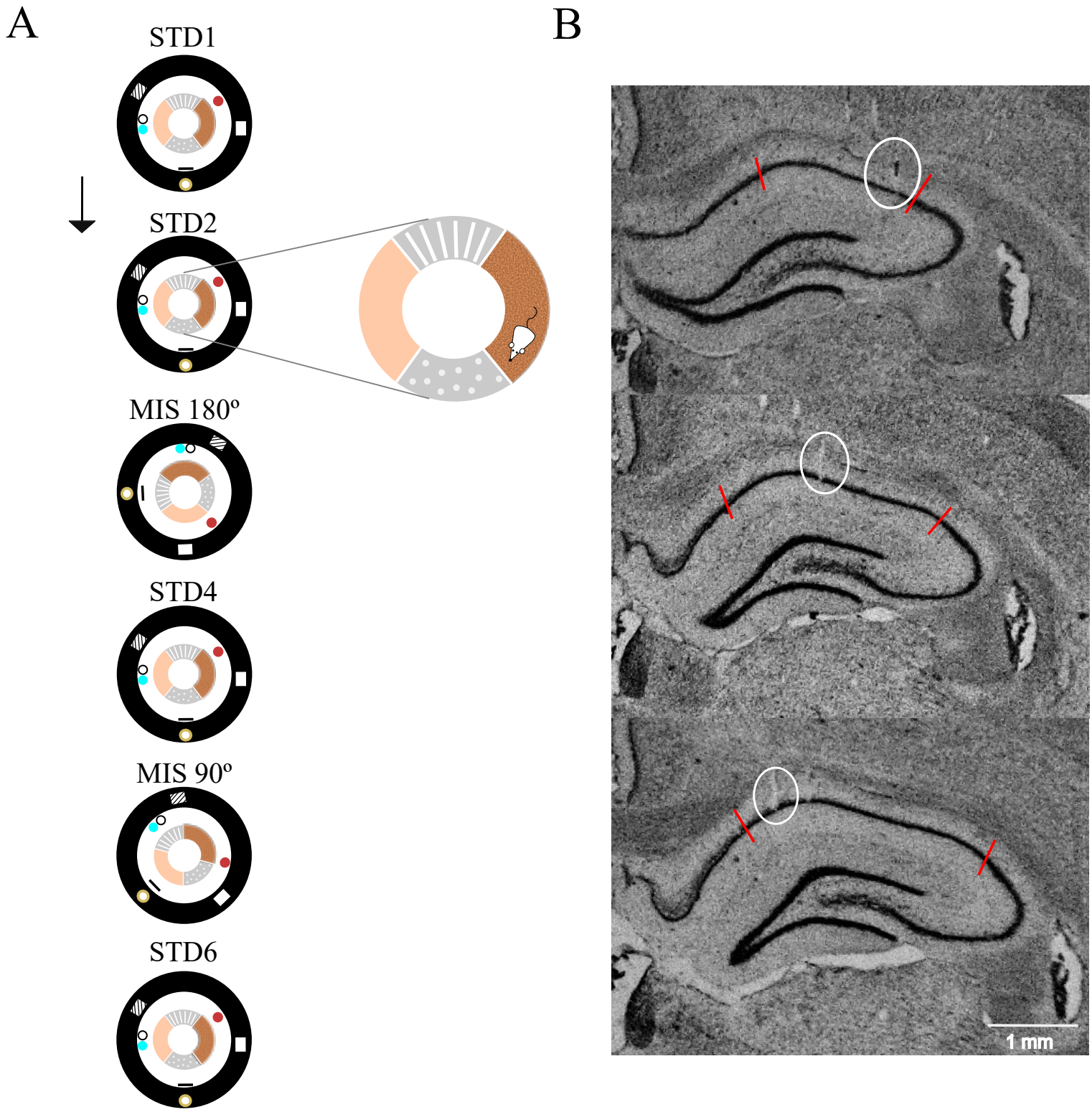

Figure 1

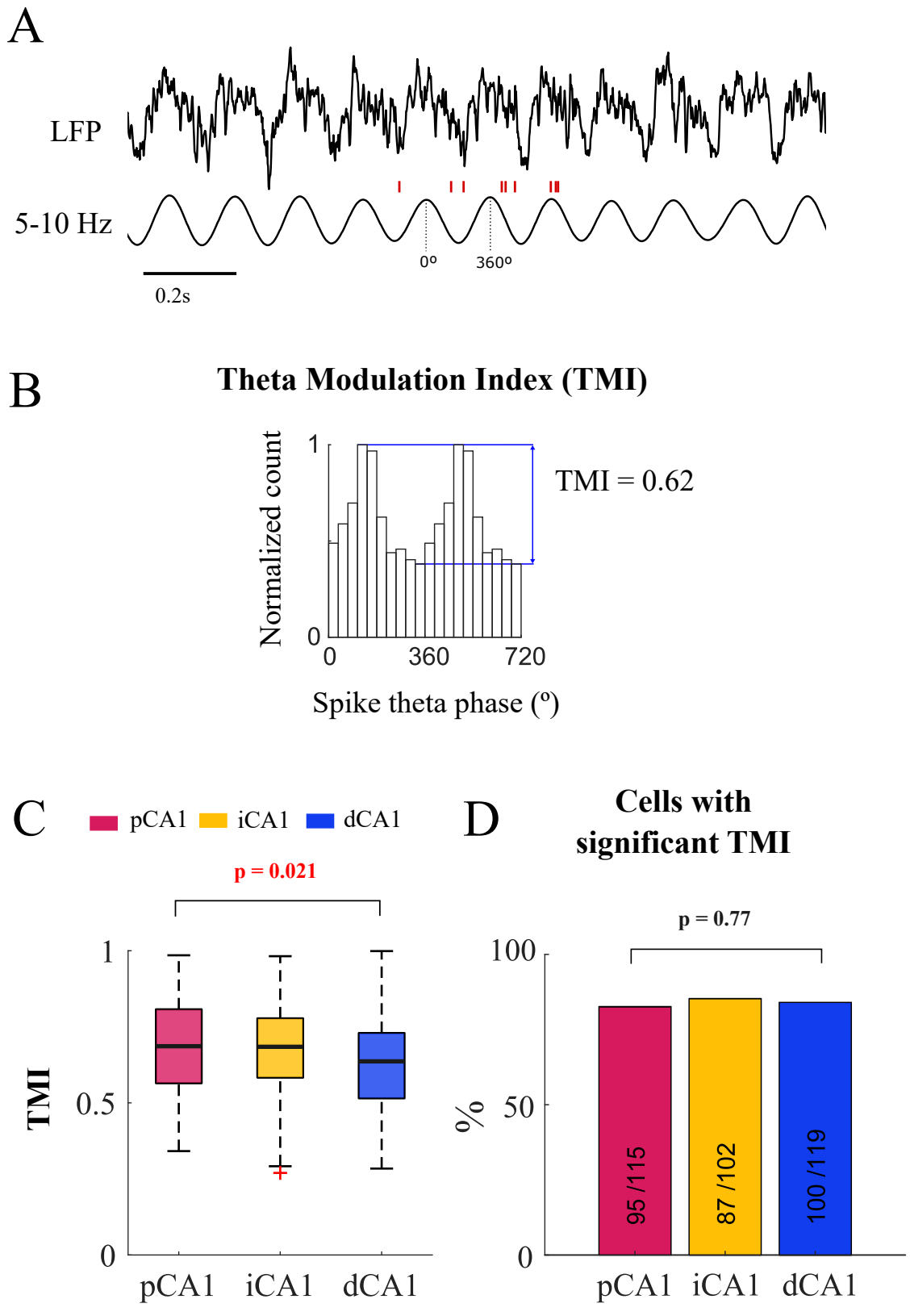
A
LFP
5-10 Hz
0º
360º
0.2s
B
Theta Modulation Index (TMI)
Normalized count
1
0
0
360
720
TMI = 0.62
Spike theta phase (º)
C
pCA1
iCA1
dCA1
p = 0.021
TMI
1
0.5
0
pCA1
iCA1
dCA1
D
Cells with significant TMI
p = 0.77
%
100
50
0
95 /115
87 /102
100 /119
pCA1
iCA1
dCA1

Figure 2

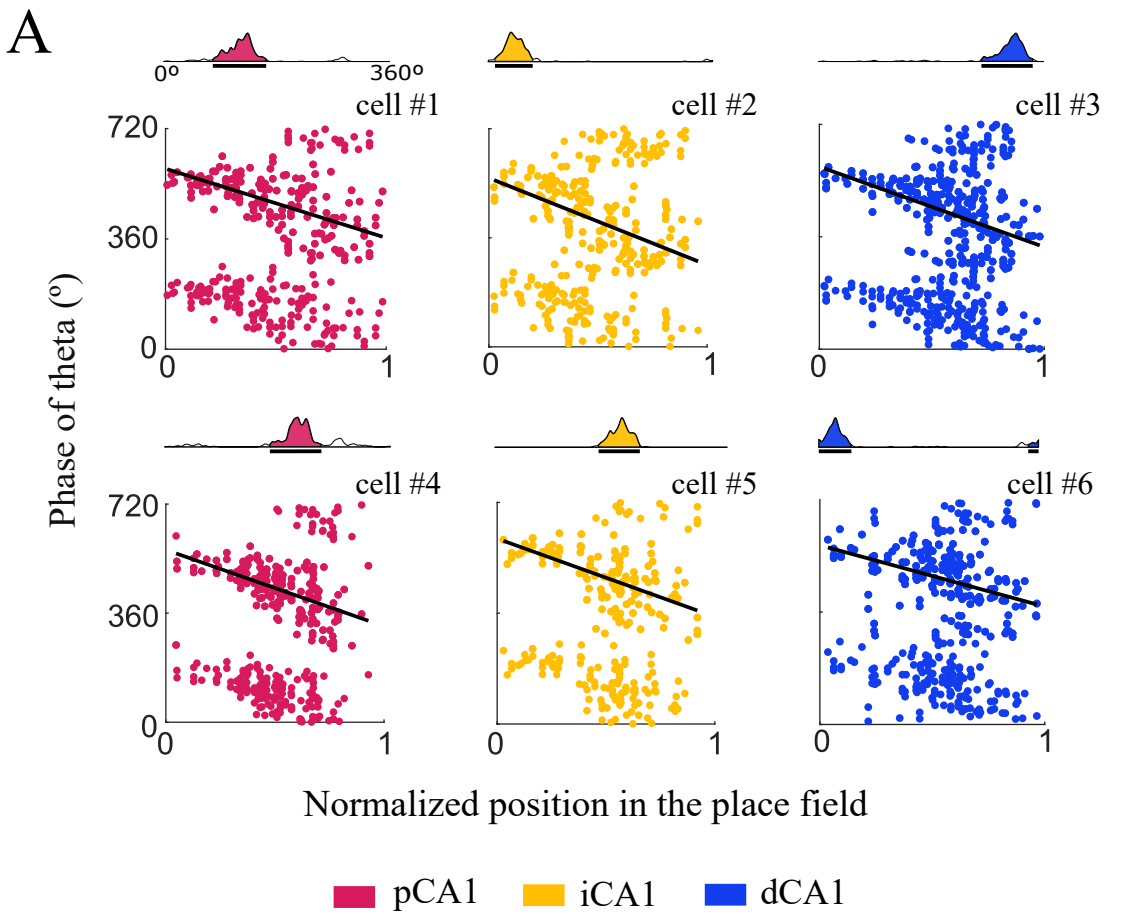
A
0º
360º
cell #1
cell #2
cell #3
cell #4
cell #5
cell #6
720
360
0
1
Phase of theta (º)
Normalized position in the place field
pCA1
iCA1
dCA1

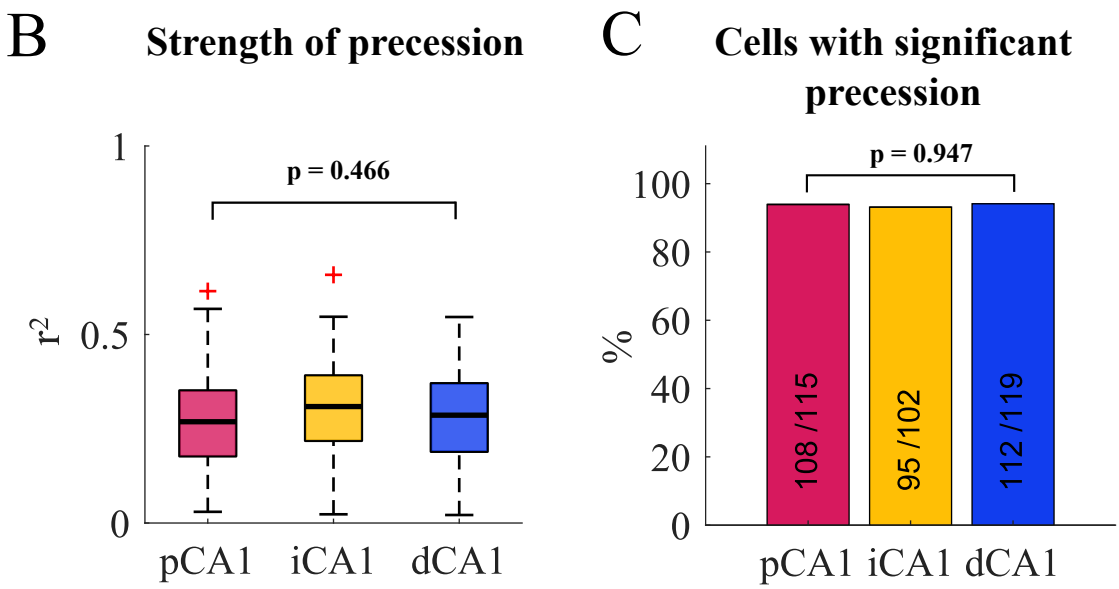
B
Strength of precession
p = 0.466
r²
1
0.5
0
pCA1
iCA1
dCA1
C
Cells with significant precession
p = 0.947
%
100
80
60
40
20
0
108 /115
95 /102
112 /119
pCA1
iCA1
dCA1

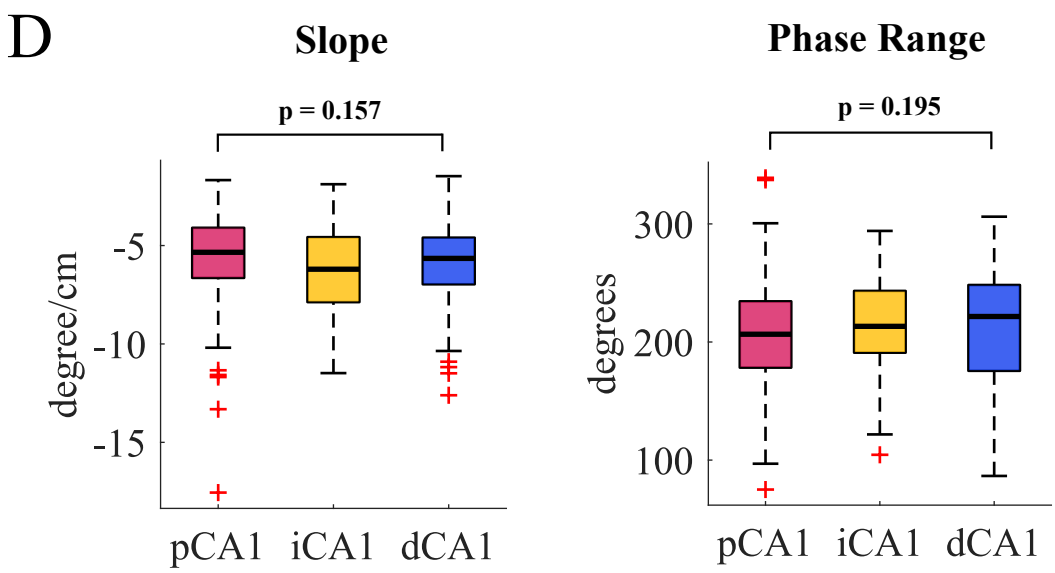
D
Slope
p = 0.157
degree/cm
-5
-10
-15
pCA1
iCA1
dCA1
Phase Range
p = 0.195
degrees
300
200
100
pCA1
iCA1
dCA1

Figure 3

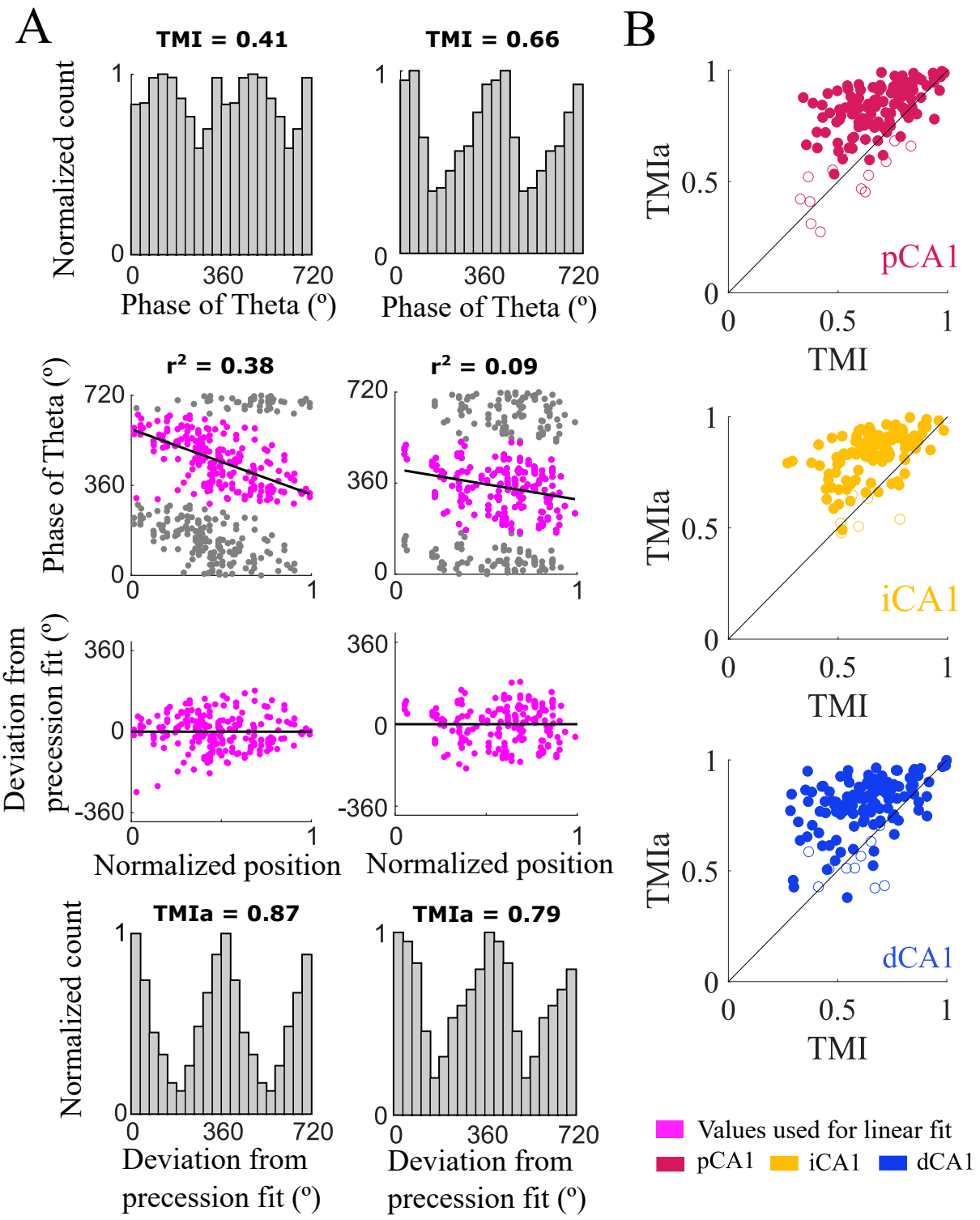
A
TMI = 0.41
TMI = 0.66
Normalized count
Phase of Theta (°)
r² = 0.38
r² = 0.09
Phase of Theta (°)
Deviation from precession fit (°)
Normalized position
TMIa = 0.87
TMIa = 0.79
Deviation from precession fit (°)
B
TMIa
TMI
pCA1
iCA1
dCA1
Values used for linear fit
pCA1 iCA1 dCA1

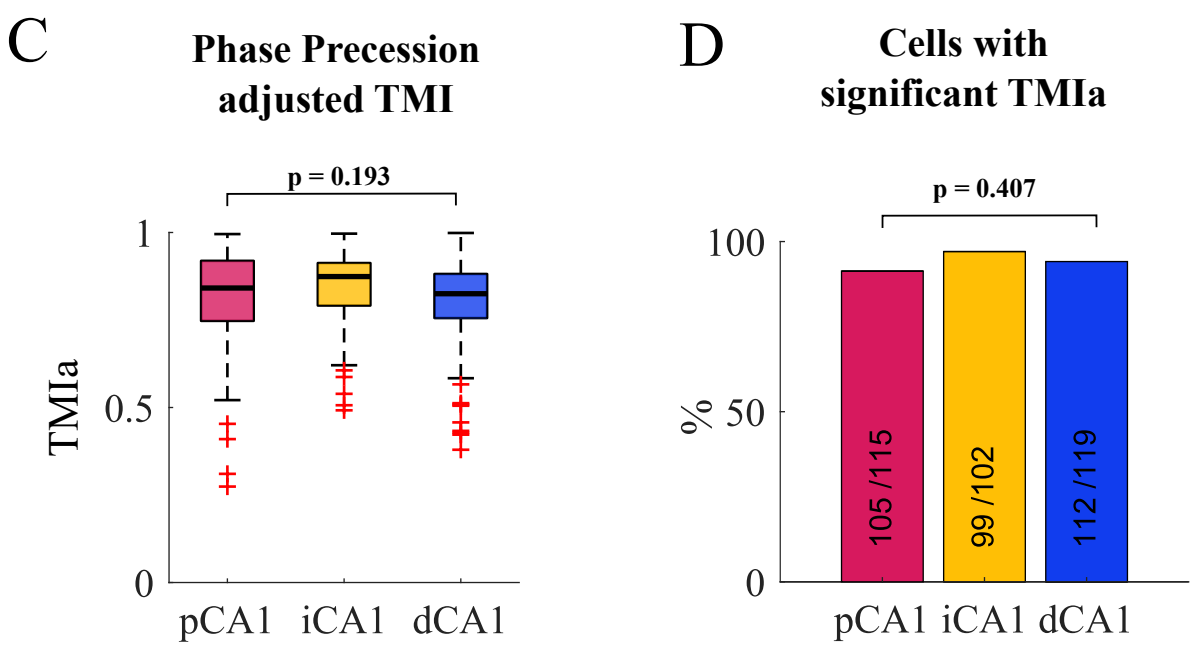
C
Phase Precession adjusted TMI
p = 0.193
TMIa
pCA1 iCA1 dCA1
D
Cells with significant TMIa
p = 0.407
%
105 /115
99 /102
112 /119
pCA1 iCA1 dCA1

Figure 4

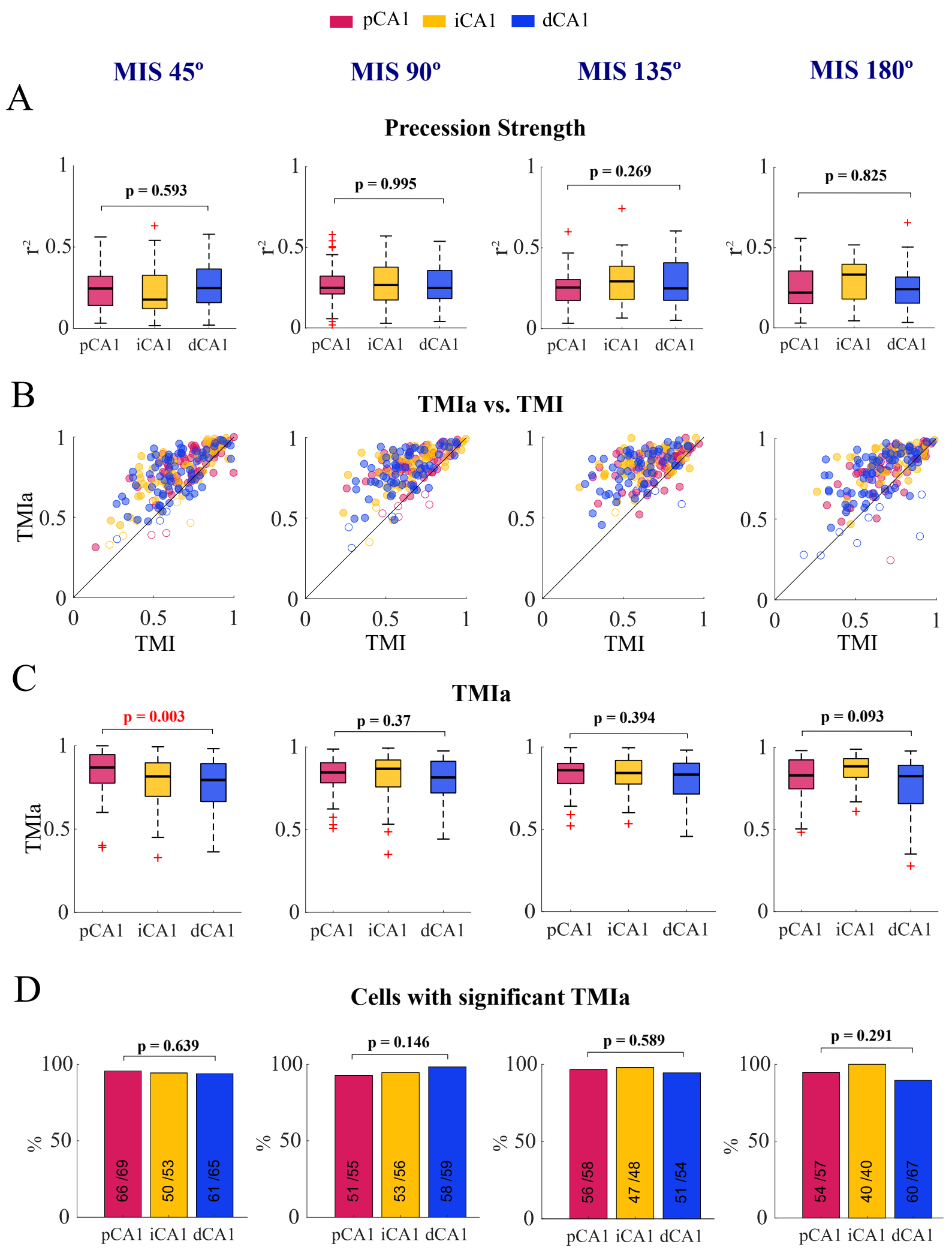
pCA1
iCA1
dCA1
MIS 45º
MIS 90º
MIS 135º
MIS 180º
A
Precession Strength
p = 0.593
p = 0.995
p = 0.269
p = 0.825
r²
B
TMIa vs. TMI
TMIa
TMI
C
TMIa
p = 0.003
p = 0.37
p = 0.394
p = 0.093
D
Cells with significant TMIa
p = 0.639
p = 0.146
p = 0.589
p = 0.291
%
66 /69
50 /53
61 /65
51 /55
53 /56
58 /59
56 /58
47 /48
51 /54
54 /57
40 /40
60 /67

Figure 5

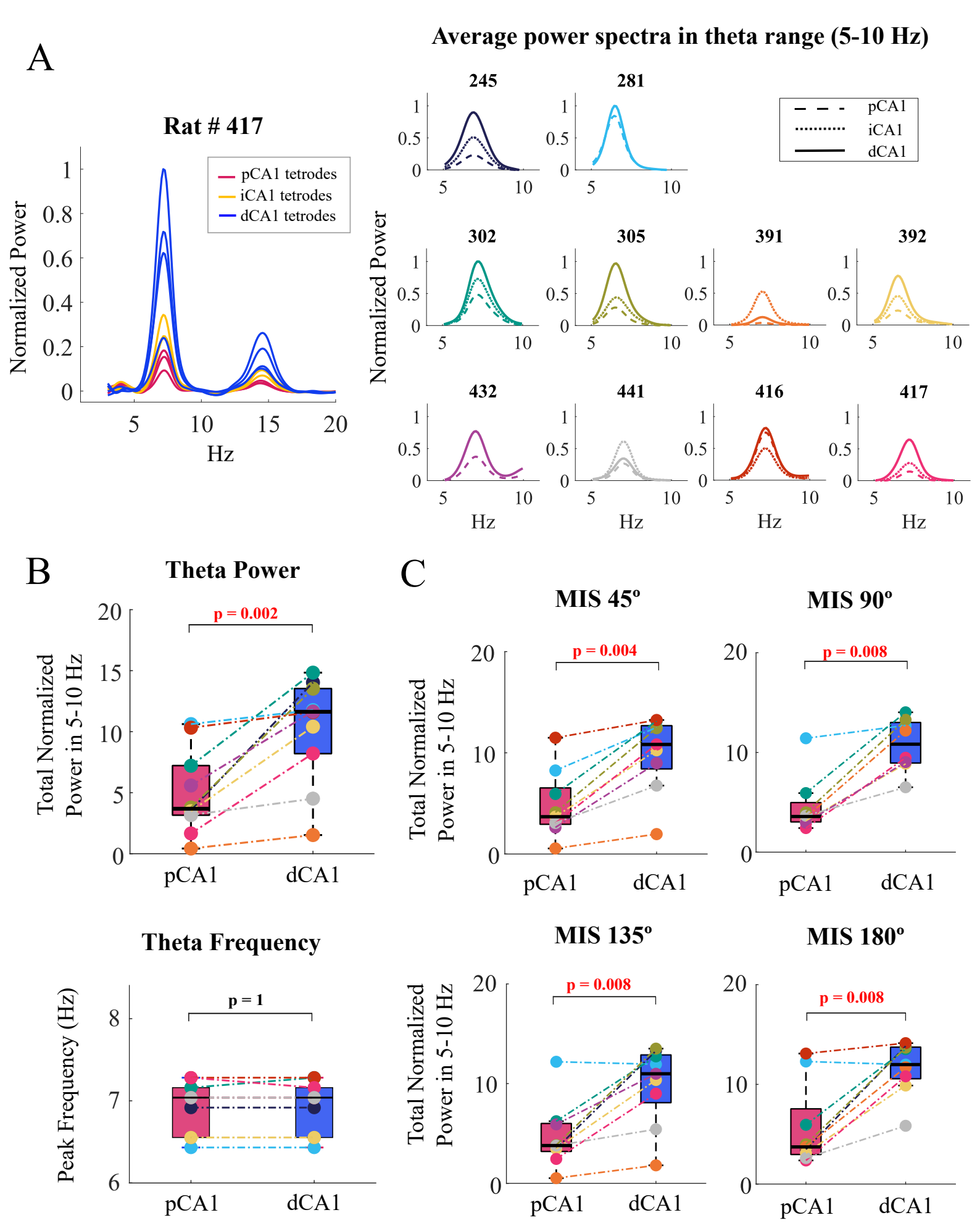
A
Rat # 417
pCA1 tetrodes
iCA1 tetrodes
dCA1 tetrodes
Normalized Power
Hz
Average power spectra in theta range (5-10 Hz)
245
281
302
305
391
392
432
441
416
417
pCA1
iCA1
dCA1
B
Theta Power
p = 0.002
Total Normalized Power in 5-10 Hz
pCA1
dCA1
Theta Frequency
p = 1
Peak Frequency (Hz)
C
MIS 45º
p = 0.004
MIS 90º
p = 0.008
MIS 135º
p = 0.008
MIS 180º
p = 0.008

Figure 6